The Report committee for Elsa Maalouf

Certifies that this is the approved version of the following report:

Numerical simulation and interpretation of sonic measurements in vertical and highly deviated wells

APPROVED BY

SUPERVISING COMMITTEE:

Supervisor:

Carlos Torres-Verdín

Hugh Daigle

Numerical simulation and interpretation of sonic measurements in vertical and highly deviated wells

by

Elsa Maalouf

Report

Presented to the Faculty of the Graduate School

of the University of Texas at Austin

in Partial Fulfillment

of the Requirements

for the Degree of

Master of Science in Engineering

The University of Texas at Austin

May, 2016

Numerical simulation and interpretation of sonic measurements in vertical and highly deviated wells

by

Elsa Maalouf, MSE

The University of Texas at Austin, 2016

SUPERVISOR: Carlos Torres-Verdín

Borehole sonic measurements are widely used to estimate formation elastic properties and to construct synthetic seismograms. However, presence of noise compromises the accuracy of sonic logs. Sonic logs are prone to errors originating from near wellbore damage or mud-filtrate invasion. Moreover, sonic logs are calculated from the numerical processing of waveforms over a wide range of receivers. Numerical processing induces errors in the sonic slowness because the slowness value is averaged over the length of the receiver array.

I apply a fast modeling method using spatial sensitivity functions to calculate sonic logs. First, I define the spatial sensitivity function for the compressional and flexural modes. Then, I apply the fast modeling in a joint inversion of shear and compressional slowness logs to mitigate noise contaminating sonic logs. Joint inversion is performed in vertical and slightly-dipping wells, to estimate layer-by-layer formation elastic and mechanical properties for isotropic and anisotropic formations.

Finally, I introduce a fast modeling procedure for compressional and flexural modes in deviated and horizontal wells. Results of the fast modeling are compared to finite-difference numerical simulations. The fast modeling of sonic borehole measurements in deviated wells can be applied in a joint inversion to estimate formation elastic and geometrical properties.

TABLE OF CONTENTS

LIST OF TABLES

LIST OF FIGURES

Chapter 1: Introduction

Sonic logging is a component of formation evaluation widely used to measure elastic properties of rocks in-situ, which are necessary for seismic interpretation and reserves appraisal. Estimating formation mechanical strength is also important for completion engineers, as they seek to determine optimal fracturing practices. Moreover, sonic logs are used to estimate seismic wavelets via synthetic seismograms. Noise present in sonic logs can bias the estimation of seismic wavelets and degrades the quality of seismic inversion-based products.

There are two sources of noise and error in sonic logs: error originating from the numerical processing of the acquired waveforms, and error due to noise in the measurement itself. The slowness-time-coherence (STC) method, widely used in the industry, is implemented by stacking the waveforms at various receivers and measuring the compressional (P) and shear (S) slowness of the formation. Because this method depends on the definition of a time coherence window, it is prone to numerical errors. Moreover, because the shear slowness is estimated from the low-frequency flexural or quadrupole mode and they have low energy, the estimation of shear slowness can be biased.

Sonic measurements in thinly laminated formations are influenced by shoulder bed effects, anisotropy, and borehole environmental effects. Such effects make the interpretation of sonic logs difficult. When layer thicknesses are smaller than the tool's receiver array length [1 to 2 m], the measurements will represent average slowness values, affecting the estimation of elastic properties.

I use an inversion-based technique to eliminate the noise contaminating the logs and improve the estimation of the formation elastic properties in vertical wells. In high-angle and horizontal (HA/HZ) wells, however, sonic log interpretation is more complex; one cannot directly apply the same inversion scheme in vertical and HA/HZ wells.

In HA/HZ wells, presence of dipping bed boundaries causes multimode interference and wave distortion. Transmitters can excite multiple modes that interfere with each other because the layers cross the borehole at a high-angle. Furthermore, three-dimensional (3D) heterogeneities make it more difficult to detect formation velocities using the same principles and methods developed for vertical wells.

In this report, I develop a fast forward model to jointly invert shear and compressional slowness in complex geometries to estimate the corresponding rock properties. Using these techniques on field data will enable the correction of slowness logs for environmental effects and processing errors. The fast forward modeling procedure will be approved using spatial sensitivity functions, that are equivalent to the Green's function of borehole acoustic measurements.

Chapter 2: Literature Review

2.1. Background on acoustics

A sonic tool is composed of a transmitter and several receivers. Figure 1 shows a diagram of a LWD tool surrounding a formation with a borehole radius *c*; *a* and *b* are the inner and outer radii of the tool's collar.

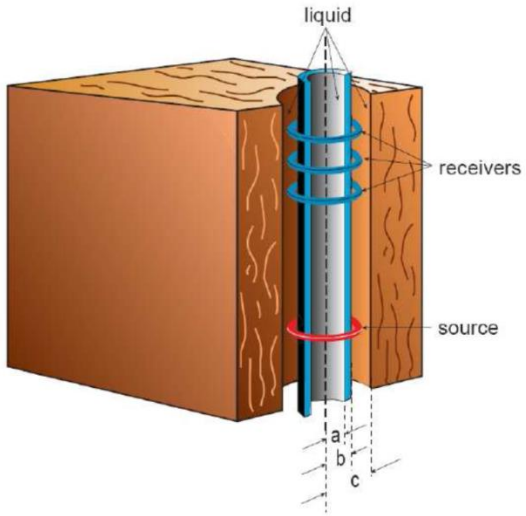

Fig. 1. Diagram of LWD tool penetrating a formation with borehole diameter c. The tool consist of a steel drill collar of inner radius a and outer radius b. (Yang et al., 2011)

Sonic tools use three types of acoustic sources: monopole, dipole, and quadrupole. Figure 2 shows a diagram of three acoustic tools in a borehole with: a monopole source (left), a dipole source (center), and a quadrupole source (right). Black and red circles represent the azimuthal wave amplitude pattern for each source, and phase difference of the waves is represented by the plus (+) and minus (-) signs.

Monopole sources emit acoustic energy in all directions from the tool axis. They can excite both surface and body waves. The propagated wave is then detected by the receivers in a receiver array. For a fast formation, where the shear velocity is larger than the borehole fluid velocity, the monopole wavetrain contains P, S, and Stoneley-wave modes. The P and S modes are non-

dispersive, whereas the Stoneley mode is dispersive, which means that its slowness varies with frequency. In slow formations, where the shear velocity is smaller than the borehole fluid velocity, the monopole wavetrain contains P and Stoneley modes. No shear head wave develops in the fluid and consequently the refracted shear waves are not detectable. The Stoneley wave is much less dispersive in slow formations.

Dipole sources emit energy in a figure-8 pattern. They generate surface waves that propagate on the borehole wall. Modern tools have two sets of dipole sources that are orthogonal. For fast and slow formations, the dipole wavetrain contains the flexural mode. The high frequency components of the flexural mode are sensitive to the borehole fluid slowness, whereas the low-frequency components asymptote to the formation shear slowness.

Quadrupole sources emit energy in clover-leaf pattern. The quadrupole wavetrain contains the screw mode. Similarly to the flexural mode, the speed of propagation of the quadrupole mode approaches the formation shear slowness below a certain low cut-off frequency. However, its cut-off frequency is higher than in the case of the flexural mode.

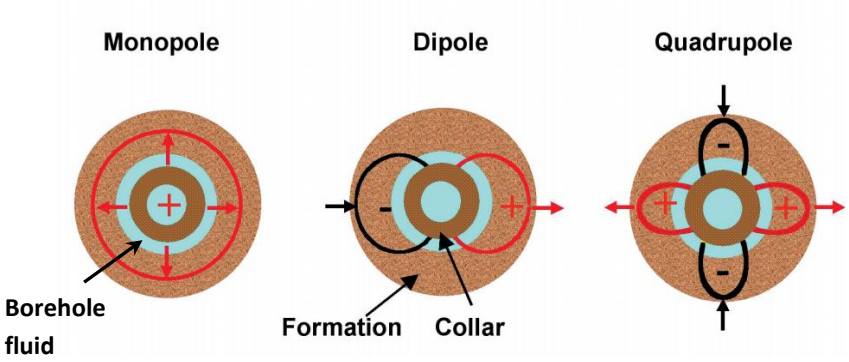

Fig. 2. Types of sonic source. From left to right: monopole, dipole, and quadrupole. Red and black circles represent the propagation of the wavefront. The inner brown ring corresponds to the drill collar of the LWD tool surrounded by the light blue borehole fluid. (Tang et al., 2003)

2.2. Simulation of acoustic modes

The source emits an acoustic pulse that propagates through the formation and is detected at the various receivers. Tang and Chang (2004) developed an analytical solution for the wave equation for formations containing a borehole surrounded by concentric layers. To obtain the waveform across the receivers, I solve the continuity equation across the borehole wall and across the boundaries of each layer. The wave potential takes into account, both, the emitted and reflected waves.

In complex geometries where layer boundaries cross the receiver array, analytical solutions do not exist. I use techniques such as finite-difference (Liu et al., 1996) to numerically simulate waveforms.

2.3. Processing techniques

Once the waveforms are registered at the receivers, they are processed to obtain the mode slowness. For non-dispersive modes, I use the STC technique to process the waveform. In this method, I calculate the coherence of the waveforms registered at the tool receivers. For a monopole source, the maximum of the coherence will correspond to the compressional or the shear slowness of the formation depending on the arrival time. Equation 2.1 gives the semblance value as defined by Kimball and Marzetta (1984):

$$\rho(s,T) = \frac{\int_T^{T+T_w} \left| \sum_{m=1}^{N} X_m(t + s(m-1)d) \right|^2 dt}{N \int_T^{T+T_w} \sum_{m=1}^{N} |X_m(t + s(m-1)d)|^2 \, dt}, \tag{2.1}$$

where X_m is the acoustic time signal at the m^{th} receiver; *N* the total number of receivers; *d* the receiver spacing, and *s* the sonic slowness; T is the center of the time window T_w.

For dispersive modes, in the frequency domain, the semblance is given by

$$\rho(s_0, f) = \frac{\left|\sum_{m=1}^{N} {X_m}^*(f) Z_0^{n-1}\right|}{\sqrt{N \sum_{m=1}^{N} {X_m}^*(f) X_m(f)}}, \quad (2.2)$$

where $Z_0 = \exp(-i2\pi f s_0 d + \varepsilon)$, with s_0 the slowness and ε the error term; * denotes the complex conjugate of the spectrum X_m, where $X_m = h_k(2\pi f) \cdot \exp(-i2\pi f s_k(n-1)d)$ with h_k the amplitude of the k^{th} wave mode, and s_k the corresponding slowness. The semblance is maximized when $s_0 = s_k$. This processing method is the weighted spectral semblance method.

2.4. Errors in sonic logs

As discussed in previous sections, the sonic response is detected at several receivers. Therefore, when multiple layers cross the receiver array, the measured slowness is averaged through the layers. In formations with thin layers, compressional and shear logs will be affected by shoulder beds (Peyret and Torres-Verdín, 2006).

Because the depth of investigation of sonic logs is approximately 0.6 m, sonic logs are sensitive to near well-bore alterations and invasion. Other sources of noise for sonic logs are: caliper variations, presence of gas in the formation, and presence of fractures (Oyler et al., 2008). In addition, processing techniques can introduce numerical errors in the calculated slowness, which will be more significant for tools with fewer receivers.

I use inversion techniques to overcome these problems and have a better interpretation of sonic logs. By jointly inverting shear and compressional logs, it is possible to obtain better estimations of the formation's elastic properties such as Poisson's ratio and Young's modulus. Numerical simulations are not suitable for inversion purposes because they are extremely time-consuming. Therefore, developing a fast forward model will enable the implementation of an inversion technique to understand and interpret sonic logs.

2.5. Fast modeling and sensitivity functions in vertical wells

2.5.1. Radial sensitivity function

The slowness of a formation is sensitive to elastic property variations in the radial direction due mud-filtrate invasion or near well bore alteration. Sinha (1997) studied the impact of five elastic properties on the flexural mode using radial sensitivity functions. Moreover, to estimate the radial profile of shear velocity, Sinha et al. (2006b) developed an inversion interpretation of the flexural mode using radial sensitivity functions.

The radial sensitivity function of a formation where elastic properties vary only in the radial direction is given by

$$G_r(r, M_r, f) = \frac{[s(r,f) - s_r(f)]/s_r(f)}{[\frac{M - M_r}{M_r}]r\Delta r}, \tag{2.3}$$

where s_r and M_r are the slowness and elastic property of the reference homogeneous formation, respectively; s is the perturbed formation slowness due to a cylindrical layer of thickness Δr and elastic property M located at position r; s is measured at the center of the receiver array by the various receivers. For dispersive modes, the value of slowness s is a function of the frequency, f. Slowness s is calculated analytically by solving the wave equation in a formation with concentric layers using a root finding technique.

The diagram in Fig. 3 shows the model used for calculating the sensitivity function at a specific location r. To obtain the sensitivity function for all the locations we translate the layer of thickness Δr in the horizontal r direction.

I calculate the radial sensitivity functions of the flexural mode to perturbation of shear slowness. I consider the slow formation given in Table 1 and the sonic tool properties given in Table 2. I use Equation 2.3 where $s(r,f)$ and $s_r(f)$ are the flexural slowness at frequency f of the perturbed and homogeneous formations, respectively. The perturbed shear velocity and the

reference shear velocity of the formation are given by M and M_r, respectively. In this example, I take a perturbation of 10%, therefore $\frac{M-M_r}{M_r} = 0.1$.

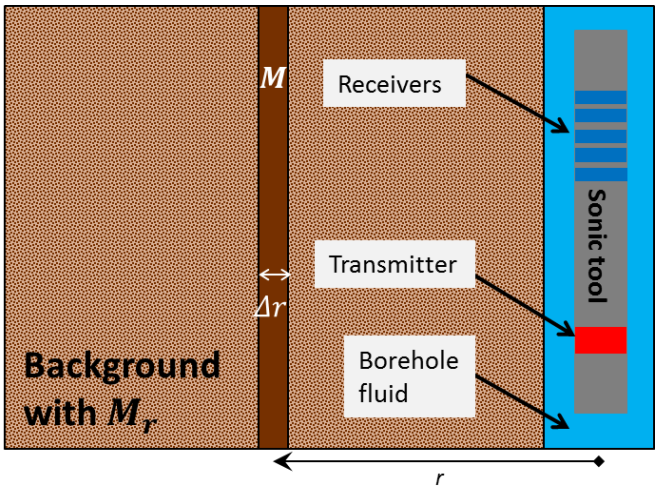

Fig. 3. Diagram of a homogeneous formation with an embedded layer perturbation in the radial direction. The formation is penetrated by a sonic tool with one transmitter and several receivers.

Figure 4 shows the calculated radial sensitivity function of the flexural mode to shear velocity for a slow formation. Formation and tool properties are given in Tables 1 and 2, respectively. Radial sensitivity functions are given at discrete frequencies from 2.5 kHz to 7 kHz. As frequency increases, the depth of investigation decreases from about 0.5 m at 2 kHz to 0.3 m at 7 kHz. Therefore, at high frequencies, the sensitivity of the flexural mode to shear velocity is high near the borehole and decreases to almost 0 at 0.3 m away from the borehole.

Compressional velocity V_p (m/s)	**3000**
Shear velocity V_s (m/s)	**1500**
Density ρ (kg/m^3)	**2500**

Table 1. Elastic properties of a homogenous slow formation.

2.5.2. Axial sensitivity function

Numerical simulation of sonic logs requires high computational time which prevents the use of inversion-based interpretation on shear and compressional slowness logs. A fast forward model using sensitivity functions was introduced by Huang et al. (2015) for the fast modeling of sonic logs. The shape of the axial sensitivity function depends on tool configuration, borehole properties, and the choice of reference medium. The axial sensitivity function of a formation where elastic properties vary only in the axial direction is given by

$$G_z(z, M_r, f) = \frac{[s(z,f) - s_r(f)]/s_r(f)}{[\frac{M - M_r}{M_r}]\Delta z}, \tag{2.4}$$

where s_r and M_r are the slowness and elastic property of the reference homogeneous formation, respectively; s is the perturbed formation slowness due to a horizontal layer of thickness Δz and elastic property M located at position z; s is measured at the center of the receiver array by the various receivers. For dispersive modes, the value of slowness s is a function of frequency, f.

Tool diameter (m)	**0.0920**
Compressional velocity: V_p (m/s)	**1650**
Shear velocity: V_s (m/s)	**400**
Density: ρ (kg/m^3)	**4452**
Number of receivers	**13**
Inter-receiver distance (m)	**0.1524**
First receiver offset (m)	**3.2766**

Table 2. Properties of the assumed sonic tool.

The diagram in Fig. 5 shows the model used for calculating the sensitivity function at a specific depth z. To obtain the sensitivity function for all the locations of the receiver array, I translate the layer of thickness Δz in the vertical, z direction. Figure 5 shows the axial sensitivity function

calculated for the slow formation given in Table 1. The axial sensitivity functions are given at discrete frequencies from 2.5 kHz to 7 kHz. The value of the sensitivity function is maximal at the center of the receiver array and is equal to zero outside the receiver array range.

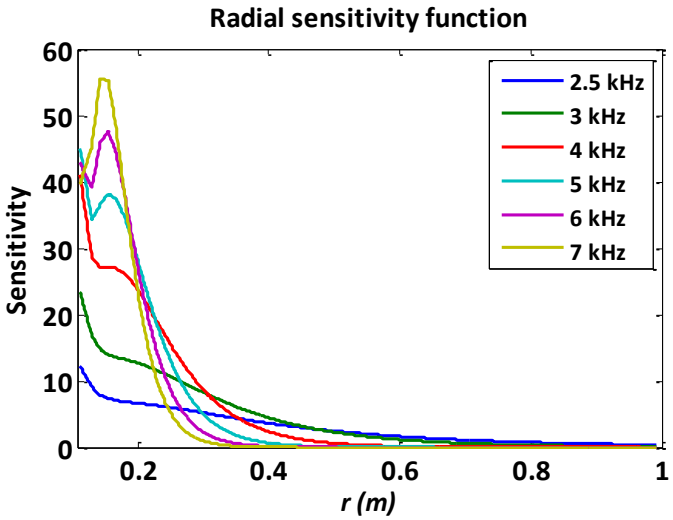

Fig. 4. Radial sensitivity functions of the flexural mode to shear velocity calculated using Equation 2.3 for a slow formation. Radial sensitivity curves are shown at 2.5, 3, 4, 5, 6, and 7 kHz. Radial distance from the borehole is given by *r (m)*.

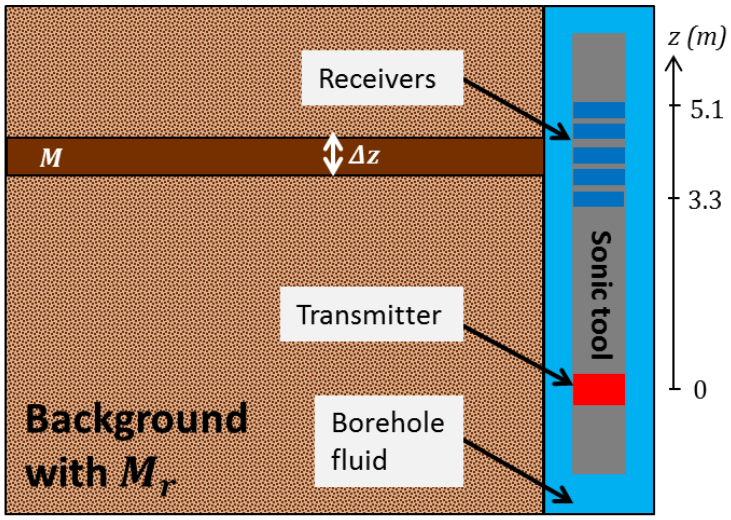

Fig. 5. Diagram of a homogeneous formation with a horizontal layer perturbation.

To avoid time-consuming numerical simulations to calculate $s(z,f)$, I use semi-analytical formulations to calculate the sensitivity functions by modeling wave propagation through a one-dimensional (1D) layered medium (Huang et al., 2015).

First, I consider a homogeneous formation with phase slowness s_r. The n^{th} receiver on the sonic tool registers a wave spectrum, X, defined as

$$X_n(f) = AZ^{(n-1)}, \tag{2.5}$$

$$Z = e^{-i2\pi f s_r d}, \tag{2.6}$$

where f is frequency, A is amplitude, and d is inter-receiver spacing.

Then, I place a thin layer of slowness s_p between two consecutive receivers at locations z_m and z_{m+1}. The receivers below receiver m will sense an up-going wave of amplitude A and a reflected wave of amplitude B that is due to wave reflection at the lower boundary of the thin layer. Similarly, receiver *m+1* will sense the up-going wave C and a reflected wave of amplitude D that is due to wave reflection at the upper boundary of the thin layer. Finally, receivers above location *m+1* will sense an up-going wave of amplitude E.

To obtain the wave amplitudes, I solve the displacement and stress continuity equations across the two layer boundaries. Because amplitude A depends on the choice of the sonic source, I normalize the system of equation by A and obtain the following system of equations

$$\begin{bmatrix} -2\pi f s_r e^{-i2\pi f s_r z_m} & -2\pi f s_p e^{-i2\pi f s_p z_m} & 2\pi f s_p e^{i2\pi f s_p z_m} & 0 \\ (2\pi f)^2 \rho e^{i2\pi f s_r z_m} & -(2\pi f)^2 \rho e^{-i2\pi f s_p z_m} & -(2\pi f)^2 \rho e^{i2\pi f s_p z_m} & 0 \\ 0 & -2\pi f s_p e^{-i2\pi f s_p z_{m+1}} & 2\pi f s_p e^{i2\pi f s_p z_{m+1}} & 2\pi f s_r e^{-i2\pi f s_r z_{m+1}} \\ 0 & -(2\pi f)^2 \rho e^{-i2\pi f s_p z_{m+1}} & -(2\pi f)^2 \rho e^{i2\pi f s_p z_{m+1}} & (2\pi f)^2 \rho e^{-i2\pi f s_r z_{m+1}} \end{bmatrix} \begin{bmatrix} B \\ C \\ D \\ E \end{bmatrix}$$

$$= \begin{bmatrix} -2\pi f s_r e^{-i2\pi f s_r z_m} \\ -(2\pi f)^2 \rho e^{-i2\pi f s_r z_m} \\ 0 \\ 0 \end{bmatrix}. \tag{2.7}$$

To calculate the values of s_r and s_p at frequency f, I use an analytical dispersion estimation method in homogeneous formations. I then solve Equation 2.7 to obtain B, C, D and E. I neglect

the contribution of reflected waves of amplitude *B* and *D* because their influence is minimal on sonic slowness. Therefore the spectrum at each receiver becomes

$$[X_1(f), X_2(f), \dots, X_m(f), X_{m+1}(f), X_{m+2}(f), \dots, X_N(f)] = [A, AZ, \dots, AZ^{(m-1)}, Ce^{-i2\pi f s_p md}, EZ^{(m+1)} \dots, EZ^{(N-1)}], \quad (2.8)$$

where *N* is the total number of receivers. Because s_r and s_p are measured by a sonic tool penetrating a fluid filled borehole, the spectrum incorporates the contribution from the borehole and tool on the sonic response. In practice, while *m* varies from 1 to *N*, the thin layer, shown in Fig. 5, moves across the receiver array.

To calculate the slowness of the formation $s(z, f)$, I process the spectrum calculated at each receiver when using the weighted spectral semblance method. Figure 6 shows the calculated axial sensitivity function of the flexural mode to shear velocity for the slow formation given in Table 1.

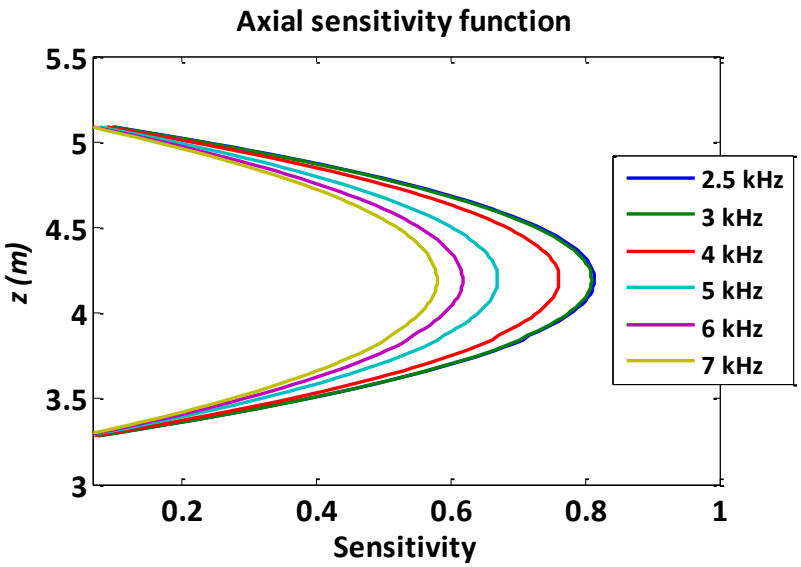

Fig. 6. Axial sensitivity functions of the flexural mode to shear velocity calculated using Equation 2.4 for a slow formation. Axial sensitivity curves are shown at 2.5, 3, 4, 5, 6, and 7 kHz. Distance from the source is given by *z* while the receiver array extends from 3.2766 m to 5.1054 m.

2.5.3. Axial-radial sensitivity function

The axial-radial sensitivity function consists of perturbing the formation in the radial and in the axial direction as shown in Fig. 7. Therefore, the perturbed volume has the shape of a toroid with a rectangular cross section, and in cylindrical coordinate the sensitivity function is given by

$$G_{rxz}(r, z, M_r, f) = \frac{[s(r, z, f) - s_r(f)]/s_r(f)}{[\frac{M - M_r}{M_r}]r\Delta r\Delta z}, \tag{2.9}$$

where s_r and M_r are the slowness and elastic property of the reference homogeneous formation, respectively; s is the perturbed formation slowness due to a mesh of volume $r\Delta r\Delta z$ and elastic property M located at position (r, z); s is measured at the center of the receiver array by the various receivers. For dispersive modes, the value of slowness s is a function of frequency, f.

Because the axial and radial sensitivity functions are uncorrelated, I calculate the axial-radial sensitivity function G_{rxz} using the cross product of both the sensitivity functions:

$$G_{rxz} = \frac{G_r * G_z}{\iint_{r,z} G_r * G_z \, rdrdz}, \tag{2.10}$$

where G_r and G_z are the radial and axial sensitivity functions, respectively. Figure 8 shows the axial-radial sensitivity map of the slow formation given in Table 1 for discrete frequencies form 2.5 kHz to 7 kHz.

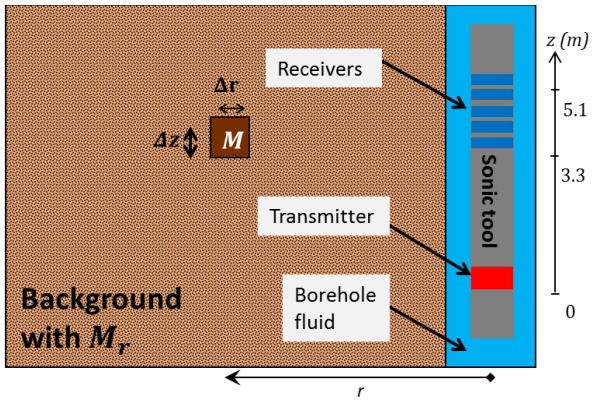

Fig. 7. Diagram of a homogeneous formation with a perturbation of radial thickness Δr and axial thickness Δz.

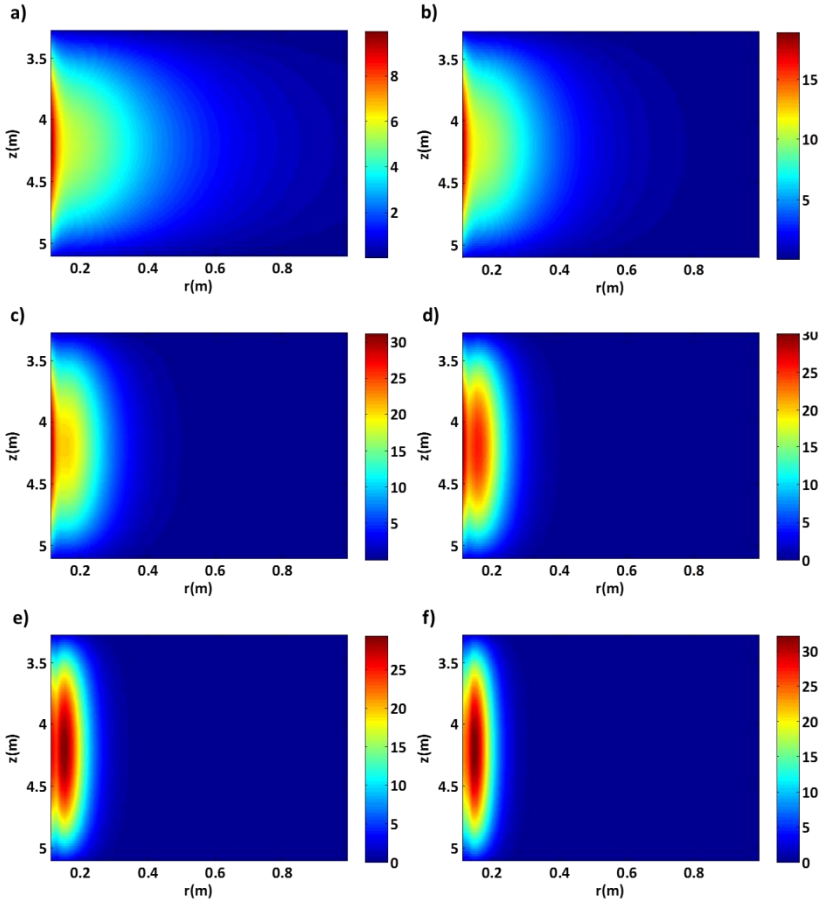

Fig. 8. Axial-radial sensitivity functions of the flexural mode to shear velocity perturbation at (a) 2.5, (b) 3, (c) 4, (d) 5, (e) 6, and (f) 7 kHz, calculated in the slow formation described in Table 1. Color scale indicates the sensitivity function value.

2.5.4. Forward model

For a formation with multiple horizontal layers, the modeled sonic slowness at a certain frequency is given by

$$s = s_r + \sum_{M_r} \sum_{z} \sum_{r} \frac{M(r,z) - M_r}{M_r} G_{rxz}(r,z,M_r)\, s_r r \Delta r \Delta z, \tag{2.11}$$

where s_r is the slowness of a reference homogeneous formation of elastic property M_r; $M(r,z)$ is the elastic property of the perturbed toroid at the location (r,z). The cross sectional area of the toroid is $\Delta r \Delta z$ and G_{rxz} is the radial-axial sensitivity function. The first sum in Equation 2.11 refers to the perturbation in the elastic properties, namely shear velocity, compressional velocity, and density, where second and third sums loop over the radial and axial domain, respectively.

2.6. Acoustics in deviated wells

Equations developed for the sensitivity functions in section 2.5 are not applicable in HA/HZ wells. The geometry can no longer be simplified to a two-dimensional (2D) problem, and the slowness is now dependent on the geometry of the formation.

Limited research has been published regarding sonic slowness in heterogeneous formations penetrated by HA/HZ wells. The propagation of sonic modes in deviated wells is more complex because of mode conversion and mode interference. The low-frequency flexural mode will be altered, which makes it difficult to extract formation shear slowness at the low-frequency asymptote (Mallan et al., 2011).

Non-dispersive modes, such as compressional and shear modes, are also affected by the presence of dipping boundaries. Borehole-guided waves interfere with the converted body waves resulting in phase discontinuity of the waveforms registered at various receivers. However, the first arrival of the P-mode is dominated by the converted P-waves in the

formation (Lin et al., 2006). It is therefore possible to simplify the 3D geometry to a 1D geometry by eliminating the borehole (Huang, 2015), as shown in Fig. 9. Figure 9 shows a formation with four horizontal layers: *L1*, *L2*, *L3* and *L4*. The sonic tool is simplified to a point source *S* and three receivers: *r1*, *r2*, and *r3*; *z1*, *z2*, and *z3* are boundary locations of the layers.

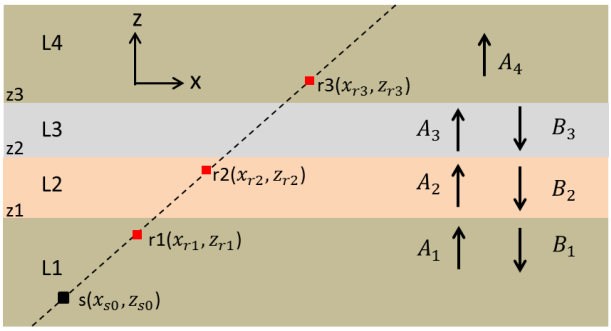

Fig. 9. Diagram of the simplified model used to simulate compressional slowness.

Through this simplified model, I calculate the waveforms measured by the receivers to estimate the first arrival of the P-mode. I assume that the shear velocity of the layers is zero because shear velocity does not contribute to the first arrival of the compressional mode. Compressional potentials are defined as

$$\phi_{A,n} = A_n e^{ik_{cn}z} e^{-ik_x x}, \tag{2.12}$$

and

$$\phi_{B,n} = B_n e^{-ik_{cn}z} e^{-ik_x x}, \tag{2.13}$$

where A_n and B_n are the amplitudes of the up-going and down-going potentials, ϕ, and $n = 1,2, \dots N$ where N is the total number of layers; k_{cn} and k_x are the wavenumbers in the z and x direction, respectively, and satisfy

$$k_{cn}{}^2 + k_x{}^2 = \frac{\omega^2}{v_{pn}^2}, \tag{2.14}$$

where $\omega = 2\pi f$ is angular frequency and v_{pn} is compressional velocity of layer n. To obtain the amplitudes, I solve the continuity equation at the boundaries. The normal displacement and the normal stress satisfy

$$u_{zn} = \frac{\partial \phi_{A,n}}{\partial z} + \frac{\partial \phi_{B,n}}{\partial z} = (ik_{cn})\big(\phi_{A,n} - \phi_{B,n}\big), \tag{2.15}$$

and

$$\sigma_{zn} = \lambda_n \frac{\partial u_{zn}}{\partial z} = \big(-\lambda_n {k_{cn}}^2\big)\big(\phi_{A,n} + \phi_{B,n}\big), \tag{2.16}$$

where λ_n is the first Lamé constant of layer n. I apply the global matrix method (Lowe, 1995) to solve for the wave amplitudes. The system to solve becomes

$$\begin{bmatrix} m_{11} & m_{12} & m_{13} & 0 & 0 & 0 \\ m_{21} & m_{22} & m_{23} & 0 & 0 & 0 \\ 0 & m_{32} & m_{33} & m_{34} & m_{35} & 0 \\ 0 & m_{42} & m_{43} & m_{44} & m_{45} & 0 \\ 0 & 0 & 0 & m_{54} & m_{55} & m_{56} \\ 0 & 0 & 0 & m_{64} & m_{65} & m_{66} \end{bmatrix} \begin{bmatrix} B_1 \\ A_2 \\ B_2 \\ A_3 \\ B_3 \\ A_4 \end{bmatrix} = \begin{bmatrix} b_0 \\ b_1 \\ 0 \\ 0 \\ 0 \\ 0 \end{bmatrix}, \tag{2.17}$$

where non-zero coefficients of the matrix are given in Table 3.

$m_{11} = ik_{c1}$,	$m_{42} = \lambda_2 {k_{c2}}^2 e^{ik_{c2}(z_2 - z_1)}$,
$m_{12} = ik_{c2}$,	$m_{43} = \lambda_2 {k_{c2}}^2$,
$m_{13} = ik_{c2} e^{ik_{c2}(z_2 - z_1)}$,	$m_{44} = -\lambda_3 {k_{c3}}^2$,
$m_{21} = \lambda_1 {k_{c1}}^2$,	$m_{45} = -\lambda_3 {k_{c3}}^2 e^{ik_{c3}(z_3 - z_2)}$,
$m_{22} = -\lambda_2 {k_{c2}}^2$,	$m_{54} = -ik_{c3} e^{ik_{c3}(z_3 - z_2)}$,
$m_{13} = -\lambda_2 {k_{c2}}^2 e^{ik_{c2}(z_2 - z_1)}$,	$m_{55} = ik_{c3}$,
$m_{32} = -ik_{c2} e^{ik_{c2}(z_2 - z_1)}$,	$m_{56} = ik_{c4}$,
$m_{33} = ik_{c2}$,	$m_{64} = \lambda_3 {k_{c3}}^2 e^{ik_{c3}(z_3 - z_2)}$,
$m_{34} = ik_{c3}$,	$m_{65} = \lambda_3 {k_{c3}}^2$,
$m_{35} = -ik_{c3} e^{ik_{c3}(z_3 - z_2)}$,	$m_{66} = -\lambda_4 {k_{c4}}^2$,
$b_0 = -e^{ik_{c1}(z_1 - z_{so})}$	$b_1 = i\lambda_1 k_{c1} e^{ik_{c1}(z_1 - z_{so})}$

Table 3. Non-zero coefficients of the matrix satisfying the continuity conditions.

The spectra in the frequency domain at each receiver are given by

$$p(r_1) = -\lambda_1 {k_{c1}}^2 \left(\frac{i}{k_{c1}} e^{ik_{c1}(z_{r1} - z_{s0})} + B_1 e^{ik_{c1}(z_{r1} - z_{s0})}\right) e^{-ik_x(x_{r1} - x_{s0})}, \tag{2.18}$$

$$p(r_2) = -\lambda_2 {k_{c2}}^2 \left(A_2 e^{ik_{c2}(z_{r2} - z_1)} + B_2 e^{ik_{c2}(z_{r2} - z_2)}\right) e^{-ik_x(x_{r2} - x_{s0})}, \tag{2.19}$$

and

$$p(r_3) = -\lambda_4 {k_{c4}}^2 \left(A_4 e^{ik_{c4}(z_{r3} - z_3)}\right) e^{-ik_x(x_{r3} - x_{s0})}. \tag{2.20}$$

I integrate the spectra at the receivers to obtain the modeled waveforms. For a source of spectrum $S(f)$, the spectra is given by

$$P(x_r, z_r, t) = \int_{-\infty}^{+\infty} \int_{-\infty}^{+\infty} S(f) p(r) e^{-i\omega t} dk_x \, df, \tag{2.21}$$

where $S(f)$ is the source spectrum. Rather than using time-consuming numerical simulations to obtain the waveforms, I use the approximated model to calculate the first arrival of the P-mode.

2.7. Sonic logs acquired in anisotropic formations

Many formations such as shale exhibit anisotropic characteristics. Transverse isotropy (TI) is commonly used to model formation anisotropy. In a transverse isotropic formation, the material elastic properties have an axis of symmetry: elastic properties are homogeneous along any transverse direction to the axis of symmetry (Plona et al., 2004). The elastic properties of a formation are defined using a stiffness tensor. The stiffness tensor, C, of a formation linearly associates the stress σ to the strain ε in the three directions of space *x*, *y*, and *z*. Similarly to Hooke's law, the nine equations relating stress to strain are written as

$$\sigma_{ij} = \sum_{k=1}^{3} \sum_{l=1}^{3} C_{ijkl} \varepsilon_{kl}, \qquad with \; i, j = 1, 2, 3. \tag{2.22}$$

Because the stress and the strain satisfy $\sigma_{ij} = \sigma_{ji}$ and $\varepsilon_{kl} = \varepsilon_{lk}$, only 6 of these equations are independent. The coefficients c_{ij} are functions of the Lamé parameters λ and μ of the formation, and the stiffness tensor, C, is given by

$$C = \begin{bmatrix} c_{11} & c_{12} & c_{13} & 0 & 0 & 0 \\ c_{12} & c_{22} & c_{23} & 0 & 0 & 0 \\ c_{13} & c_{23} & c_{33} & 0 & 0 & 0 \\ 0 & 0 & 0 & c_{44} & 0 & 0 \\ 0 & 0 & 0 & 0 & c_{55} & 0 \\ 0 & 0 & 0 & 0 & 0 & c_{66} \end{bmatrix}, \tag{2.23}$$

where for isotropic formations, $c_{11} = c_{22} = c_{33} = K + 4/3\mu$, $c_{44} = c_{55} = c_{66} = \mu$, $c_{12} = c_{13} = c_{23} = c_{33} - 2c_{55}$, with K and μ the bulk and shear modulus parameters. For TI formations, $c_{11} = c_{22} = K + 4/3\mu$, $c_{44} = c_{55} = c_{66} = \mu$, $c_{12} = c_{13} = c_{23} = c_{11} - 2c_{66}$.

In the case of isotropic formations, sonic tools can measure compressional velocity $v_p = \sqrt{\frac{c_{33}}{\rho}} = \sqrt{\frac{\lambda+2\mu}{\rho}}$, and shear velocity $v_s = \sqrt{\frac{c_{44}}{\rho}} = \sqrt{\frac{\mu}{\rho}}$.

However, in anisotropic formations, the compressional and shear velocities measured by the sonic tool no longer satisfy these equations. Daley and Hron (1977) developed analytical solutions to provide equivalent isotropic shear and compressional velocities for TI formations. These velocities can be measured by the sonic tool and are referred to as quasi-compressional and quasi-shear velocities.

The solution of the wave equation for an anisotropic formation has three solutions for velocity: one quasi-longitudinal (quasi-compressional velocity: v_{p-qv}), one transverse (horizontal shear velocity: v_{SH}) and one quasi-transverse (vertical shear velocity: v_{s-qs}) . In formations where the axis of symmetry of anisotropy is at an angle ϑ from the borehole, the quasi-compressional and quasi-shear velocities are functions of the stiffness parameters $[c_{11}, c_{13}, c_{33}, c_{44}, c_{66}]$ (Chi and Tang, 2003), and are given by

$$v_{s-qs} = \left[c_{11}sin^2(\vartheta) - c_{33}cos^2(\vartheta) + c_{44} - \sqrt{M}\right]^{0.5}(2\rho)^{-0.5}, \quad (2.24)$$

$$v_{p-qv} = \left[c_{11}sin^2(\vartheta) - c_{33}cos^2(\vartheta) + c_{44} + \sqrt{M}\right]^{0.5}(2\rho)^{-0.5}, \quad (2.25)$$

and

$$v_{SH} = [c_{66}sin^2(\vartheta) + c_{44}cos^2(\vartheta)]^{0.5}(\rho)^{-0.5}, \quad (2.26)$$

where, $M = [(c_{11} - c_{44})sin^2(\vartheta) - (c_{33} - c_{44})cos^2(\vartheta)]^2(\rho)^{-0.5}$, and ρ is the density of the formation. Therefore, v_{p-qv} is the velocity of the compressional head wave along the borehole axis and registered at the receivers; v_{p-qv} and v_{SH} are the low-frequency asymptote of both flexural waves propagating along the borehole axis and measured using orthogonal dipoles (Sinha et al., 2006a; He et al., 2010).

Chapter 3: Method

3.1. Introduction

Well logging can be performed at the time of drilling using logging-while-drilling (LWD) tools or after drilling using wireline tool. These tools have different configurations and different elastic and geometrical properties. The sonic modes and the sonic response will differ depending on the type of tool used. For a given tool configuration, we can construct spatial sensitivity functions of borehole sonic modes for fast modeling compressional, shear, and Stoneley logs in vertical wells penetrating horizontal layers. The fast model will take into account any variations of properties in the radial direction due to invasion or wellbore alterations. An example of such radial variations is shown in Fig. 10. The gray rectangle on the left represents the sonic tool with one transmitter at the bottom and 6 receivers at the top; R_{bh} is the borehole radius. The formation on the left has four horizontal layers with velocities: v_1, v_2, v_3, and v_4. Velocities near the borehole change due to invasion or wellbore damage.

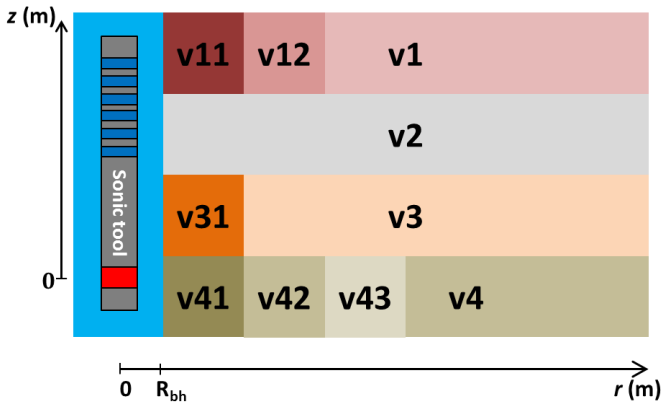

Fig. 10. (Left) A sonic tool with one transmitter (red) and 6 receivers (blue) in a borehole of radius R_{bh}. (Right) Formation with four horizontal layers.

In thinly laminated formations, where the layer thickness is smaller than the tool receiver array, sonic logs are affected by layer boundaries. These averaging effects will introduce errors when

estimating elastic properties from sonic logs. By applying a fast forward model, sonic logs can be jointly inverted to accurately estimate formation elastic properties. Because most shaly formations exhibit vertical transverse isotropy, analyzing the Stoneley log allows the detection of anisotropy in a rock. Inverting the Stoneley log allows the extraction of additional anisotropic stiffness parameters of the rock (Sinha et al., 2006a).

3.2. Fast modeling of sonic logs in vertical wells

In this section, I implement the fast simulation of compressional, shear, and Stoneley logs in vertical wells using both LWD and wireline tools.

LWD and wireline tools have different geometries which will affect sonic modes. In wireline logging, the modes used to extract shear and compressional logs are the low-frequency flexural mode and the compressional mode, respectively. In LWD, however, the flexural mode can no longer be used to estimate shear slowness. Presence of a steel drill collar in LWD tools give rise to tool modes that interfere with the flexural mode at low-frequency. The flexural mode is inadequate in sonic LWD interpretation. Therefore, we typically use the low-frequency of the quadrupole mode to obtain shear slowness with LWD tools (Sinha et al., 2009).

For this reason, for wireline tools, I calculate sensitivity functions of compressional, flexural, and Stoneley mode. For LWD tools, I calculate sensitivity functions of the compressional, quadrupole, and Stoneley modes. Another difference between wireline and LWD tools is the receiver array length: wireline tools have larger receiver arrays than LWD tools. A larger receiver array length means that the slowness of the layers will be averaged over a wider distance while smaller receiver arrays will increase the vertical resolution of the measurement. To better simulate the tool response, the sensitivity function will take into account the length of the receiver arrays.

The sensitivity function not only depends on tool geometry, but also on the reference background. Therefore, to perform fast forward modeling of a model with thin layers, we need

to adaptively select a sensitivity function at each depth. The selection of the function will depend on the formation slowness at that depth.

For the fast forward model, two cases of laminated formations can be considered:

- Formations with no invasion with isotropic or anisotropic layers: in this case we only need a 1D axial sensitivity function.
- Formations with invasion: In these formations the slowness varies radially due to changes in fluid properties. In this case, we need 2D axial-radial sensitivity functions.

To verify that the model is robust, I compare the results obtained with numerical simulations. The simulation is carried out as follows:

1. Define the earth model and build the sonic tool.
2. Use a finite-difference method to simulate sonic waveforms.
3. Use the STC method to extract compressional slowness.
4. Use a 2D finite element method (Matuszyk et al., 2013) to simulate the spectrum at different frequencies.
5. Add tool attenuation to minimize the effect of tool modes in the case of LWD tools. (Matuszyk et al., 2010).
6. Obtain the flexural or quadrupole dispersion curve using a spectral semblance processing technique (Nolte and Huang, 1997).
7. Correct for slowness shift of the quadrupole mode in the low-frequency limit for the case of LWD tools (Zhang et al., 2010).

Figure 11 describes the numerical simulation and fast forward modeling procedures.

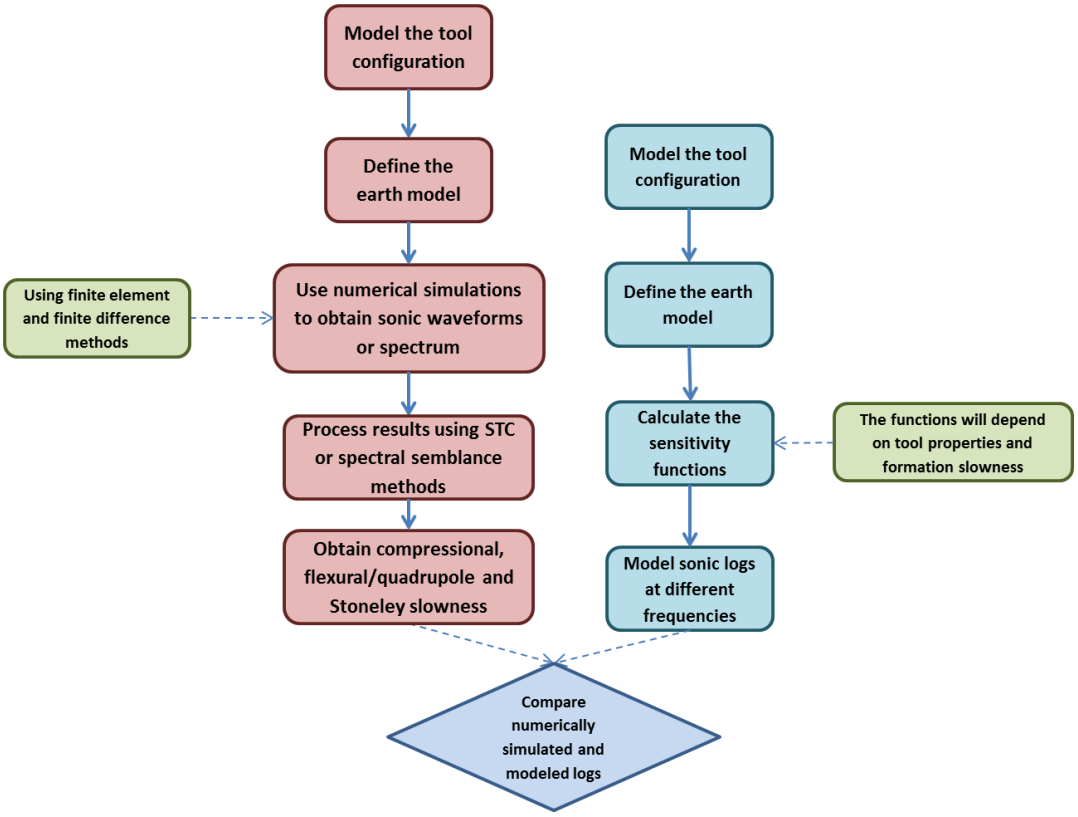

Fig. 11. Diagram showing the steps followed to simulate sonic logs in vertical wells.

3.3. Inversion of shear and compressional logs in vertical wells

3.3.1. Joint inversion

I jointly invert shear and compressional slowness logs to estimate formation elastic properties in thinly laminated formations. Synthetic logs examined have thin layers with large contrasts in slowness properties for both fast and slow formations.

The joint inversion of P and S slowness logs are performed using the axial sensitivity function and forward model given in Equations 2.4 and 2.11. To perform the joint inversion, I first define the parameters L and N as a function of compressional velocity (v_p) and shear velocity (v_s),

where $L = v_s^2$ and $N = v_p^2 - 2v_s^2$. Next, I build the cost function $e(m) = \|f(m) - d\|_2^2$, where $m = [N_1 \dots N_{n_t}, L_1 \dots L_{n_t}]$ and n_t is the number of layers; $d = [\Sigma p, \Sigma s]$, where Σp and Σs are the numerically simulated logs; $f(m) = [s_p(m), s_s(m)] = [s_1(m) \dots s_T(m)]$, where s_p and s_s are the compressional and shear slowness logs modeled using the sensitivity function and T is the total number of data. Finally, I use the Levenberg-Marquardt nonlinear least-squares method to minimize the cost function (Aster et al., 2005). To apply the Levenberg-Marquardt method, I build the Jacobian matrix $J(m)$ as

$$J(m) = \begin{bmatrix} \frac{\partial s_1}{\partial m_1} & \cdots & \frac{\partial s_1}{\partial m_n} \\ \vdots & \ddots & \vdots \\ \frac{\partial s_T}{\partial m_1} & \cdots & \frac{\partial s_T}{\partial m_n} \end{bmatrix}. \tag{3.1}$$

The model vector m is calculated iteratively, and at iteration k I calculate $m_{k+1} = m_k + \Delta m_k$, where Δm_k is the solution of the system of equations

$$\begin{bmatrix} J_k \\ \alpha I \end{bmatrix} \Delta m_k = \begin{bmatrix} d - f(m_k) \\ 0 \end{bmatrix}, \tag{3.2}$$

where I is the identity matrix and α is updated at each iteration to ensure convergence.

3.3.2. Examples

I consider a fast, homogeneous formation penetrated by an 8-in vertical borehole. The LWD tool is rigid and assumed to be centered in the borehole. Table 4 shows the properties of the tool used to simulate logs. Figure 12a shows the sonic slowness logs of a thin layered horizontal formation. The true and inverted properties of the layers are shown in green and red, respectively. Figure 12b shows the true and inverted shear and bulk modulus, respectively. I calculate the uncertainty of inversion products by adding Gaussian noise to the synthetic logs used in the inversion. The relative uncertainty between the true slowness parameters and the inversion result is below 3%.

The second synthetic case considered includes vertical transverse isotropy (VTI). In VTI formations, the vertically and horizontally polarized shear waves are different. By applying the

joint inversion described in the previous paragraph, we only estimate the vertical shear and compressional slowness of the thin layers.

Collar outer radius (m)	**0.0857**
Collar inner radius (m)	**0.0254**
Number of receivers	**12**
Inter-receiver distance (m)	**0.1524**
First receiver offset (m)	**2.13**

Table 4. Assumed LWD tool properties.

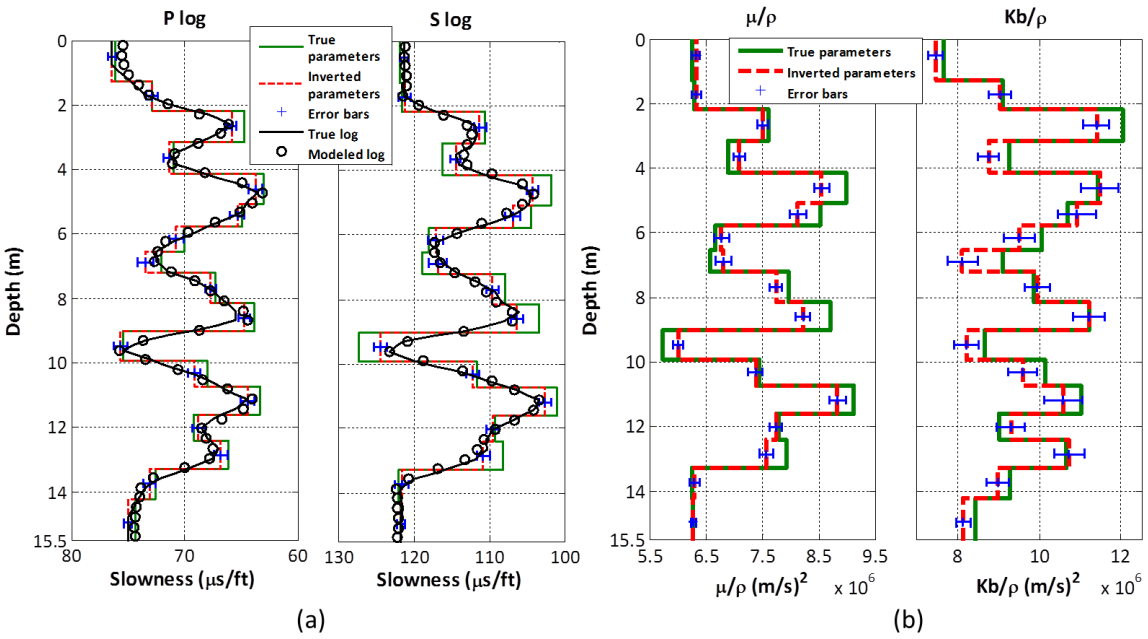

Fig. 12. Joint inversion result for the 17-layer formation: (a) P and S slowness and (b) elastic properties; μ and K_b are the shear and bulk moduli, respectively, and ρ is the density. The curves are simulated logs where circles represent modeled logs. Continuous and dashed blocky lines with error bars are the true and inverted (a) slowness and (b) elastic properties.

The low-frequency Stoneley log is predominantly sensitive to the horizontally polarized shear wave (Yang et al., 2011). Therefore, the Stoneley log allows the detection of anisotropy in the

layers. I invert the low-frequency Stoneley log to estimate the horizontal shear slowness using the sensitivity function method.

I modify the previous 17-layer formation shown in Fig. 9 by introducing anisotropy to layers 5, 8, 11, and 15 at depths 3 m, 6 m, 9 m, and 11 m, respectively. Shear and compressional slowness logs are not affected by the presence of anisotropy. However, the Stoneley log is sensitive to horizontal shear slowness. In layers 5, 8, 11, and 15, the vertical and horizontal shear slownesses are different. Figure 13a shows the Stoneley logs for the isotropic and VTI cases. To estimate the horizontal shear of the formation, I invert the Stoneley log using the axial sensitivity method. Figure 13b shows the corresponding inversion results. The average relative error of the estimation is below 2.1%. Because the logs measured by the LWD sonic tool are averaged over several layers, this method increases the vertical resolution of the logs by a factor of 2.4.

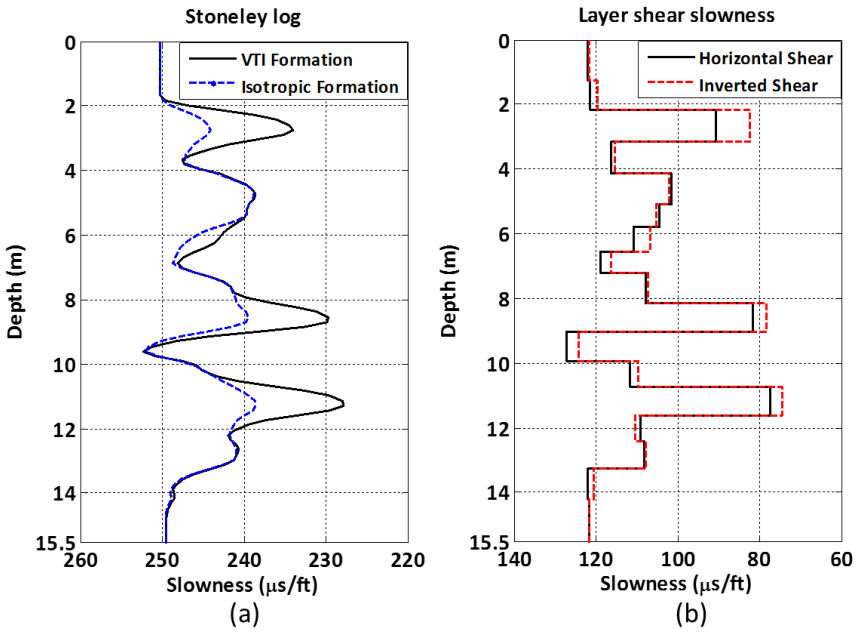

Fig. 13. Inversion of the Stoneley log using axial sensitivity functions. Dashed and continuous lines in (a) correspond to the isotropic and VTI cases, respectively. Continuous and dashed blocky lines in (b) are the true and inverted horizontal shear slowness, respectively.

3.4. Application of the axial sensitivity function to field cases

3.4.1. Introduction

Sonic logs are usually contaminated with spikes and noise. Some methods to remove noise include: using filters and reprocessing sonic waveforms, and reproducing sonic logs via effective medium theories (Sayar and Torres-Verdín, 2015). However, filtering and reprocessing sonic waveforms is time-consuming, and effective medium theories are not always practical because they provide non-unique results. In this chapter, I propose a new technique for removing noise in shear and compressional logs by applying the sensitivity function in a joint inversion of shear and compressional logs (Huang and Torres-Verdín, 2016).

3.4.2. Correction of sonic logs in the Deep Water Gulf of Mexico

One of the major issues affecting sonic measurements are changes in borehole size. These situations can generate noise and spikes, especially in shear logs. Moreover, compressional and shear logs are sensitive to fractures and gas in the mud or formation because the amplitude of the sonic modes is lower, thus making its detection more difficult (Souder, 2002). The logs will show a sharp deflection due to the high transit time caused by the presence of gas. This deflection is what is usually referred to as cycle skipping. Cycle skipping occurs when the first compressional cycle is too low to be detected at the near receiver (Ellis and Singer, 2007). Therefore, a rapid fluctuation in the compressional log is a sign of cycle skipping.

Sonic noise can be removed by treating spikes as outliers in a joint inversion of shear and compressional logs using the axial sensitivity function method as the fast forward model. I apply this method to sonic logs acquired in the Deep Water Gulf of Mexico with very noisy shear slowness, in formations that are water or light-hydrocarbon saturated. To simulate the presence of spikes, I add additional non-Gaussian biased noise to the field data. Prior to the inversion, I define layer bed-boundaries using high resolution gamma ray and density logs. The workflow for correction of shear and compressional logs is shown in Fig. 14.

3.4.3. Forward model of the shear and compressional slowness

For formations with multiple horizontal layers, the forward model for sonic slowness is given by

$$s_i(d) = s_{ri}(d) + \sum_z \frac{M(z)-M_{ri}(d)}{M_{ri}(d)} G(z, M_{ri})\, s_{ri}(d)\Delta z, \tag{3.3}$$

where $s_i(d)$ is slowness of the formation at depth d; $M_{ri}(d)$ is a reference elastic property whose value must be chosen close to the average value of M in the vicinity of depth d, such that $(M(z) - M_{ri}(d))/M_{ri}(d) \ll 1$; $s_{ri}(d)$ is the slowness corresponding to the reference homogenous formation with elastic property $M_{ri}(d)$; $M(z)$ is the value of M, at receiver location z; Δz is the inter-receiver distance used to construct the sensitivity function $G(z, M_{ri})$; and i denotes either the shear or compressional mode. As long as $(M(z) - M_{ri}(d))/M_{ri}(d) \ll 1$, $G(z, M_{ri})$ is independent of the choice of M_{ri} for both the shear and compressional modes.

3.4.4. Joint inversion

To perform the joint inversion, I first define two model parameters, *L* and *N*, as functions of Lamé's parameters λ and μ, and the density (ρ) of the formation, namely, $L = \mu/\rho = v_s^2$, $N = \lambda/\rho = v_p^2 - 2v_s^2$. By imposing a positivity constraint of model parameters L and N, I ensure that the ratio of compressional to shear velocity is always greater than $\sqrt{2}$. I then invoke the quadratic cost function $e(m) = \|f(m) - d\|_2^2$, where $m = [N_1 \dots N_{n_t}, L_1 \dots L_{n_t}]$, with n_t the total number of layers, $d = [\Sigma_p, \Sigma_s]$ where Σ_p and Σ_s are the numerically simulated logs or the field measured logs, and $f(m) = [s_p(m), s_s(m)]$, where s_p and s_s are the compressional and shear slowness logs, respectively, modeled using Equation 3.3. Finally, I use the Levenberg-Marquardt method to minimize the cost function.

The inversion method is applied to noisy shear and compressional sonic logs acquired in the Deep Water Gulf of Mexico. First, I define layer boundaries using the gamma ray (GR), density, shear slowness, and compressional slowness logs. Then, I calculate the initial estimates for L and N from the average values of shear and compressional slowness within each layer.

Figure 15 shows the results of applying the correction algorithm on 4 sections of approximately 100 ft in the Deep Water Gulf of Mexico. The first track corresponds to the caliper variations of the formation that has a 12 in borehole diameter. Caliper variability introduces uncertainty in the sonic logs that manifest as spikes and shifts in the readings of slowness. The second and third tracks are the GR and density logs, respectively. Horizontal red dashed lines in track 2 and track 3 represent the location of layer boundaries. The last two tracks are the compressional and shear slowness logs. Black logs are field measurements while red and blue logs are corrected compressional and shear logs, respectively calculated from the joint inversion algorithm. Dashed red and blue blocky logs are inverted true layer slownesses. Comparison of field logs (black) to inverted logs (red and blue) show that the spikes are mitigated and that the sonic logs are smoothed when using the joint inversion algorithm.

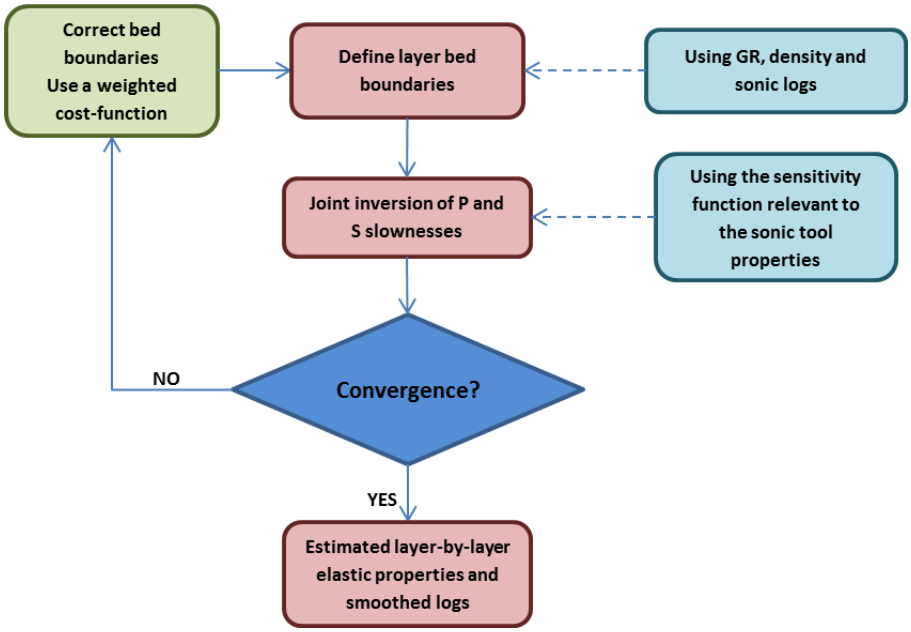

Fig. 14. Diagram showing the steps for the mitigation of noise in sonic logs.

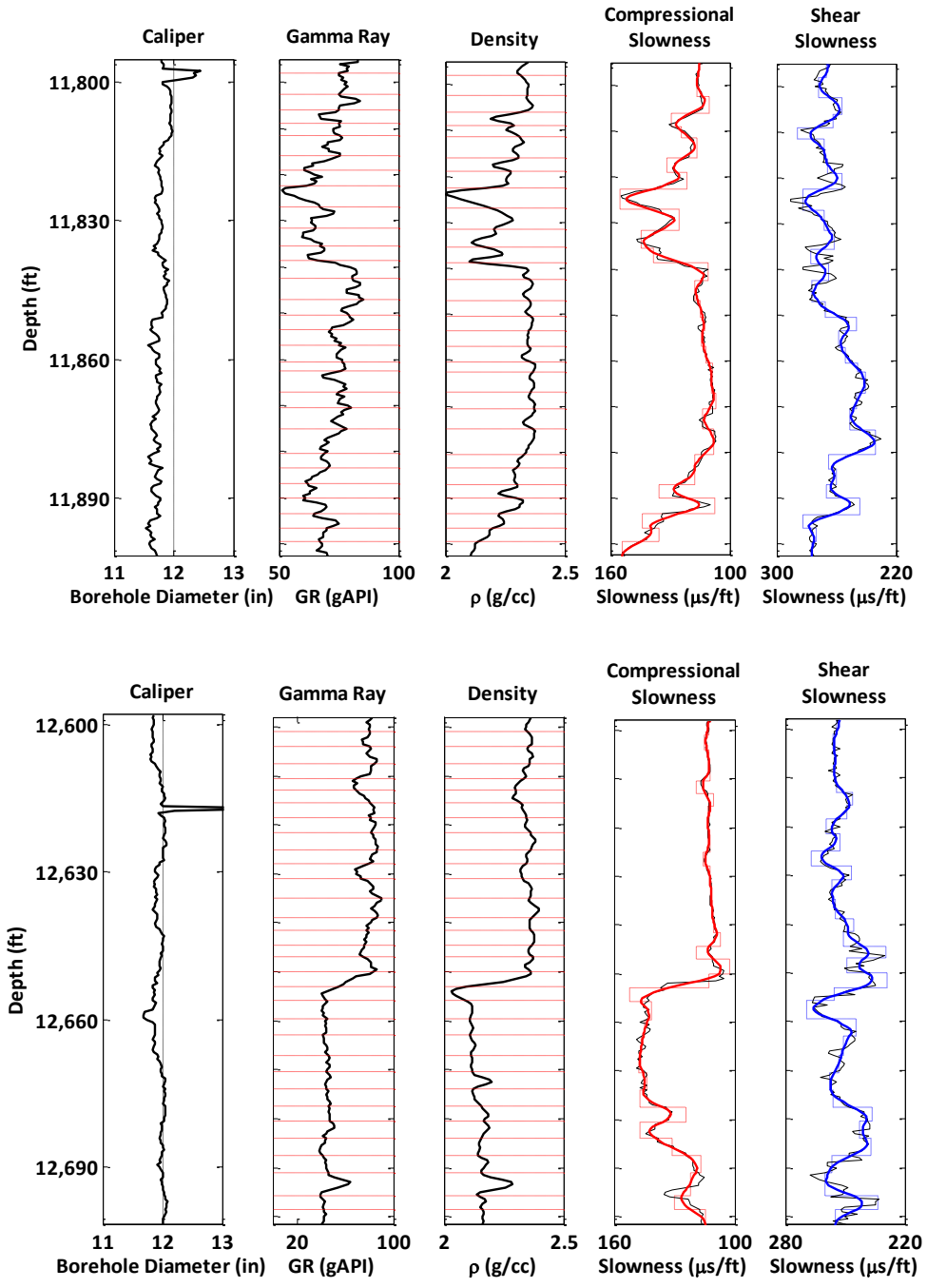

Fig. 15. (From left to right) Caliper, gamma ray, density, compressional slowness, and shear slowness logs. Red horizontal dashed lines identify the locations of bed boundaries. The second and third tracks compare noisy field logs (black) to predicted logs (blue). Dashed blocky lines with error bars describe inverted layer-by-layer slownesses of the formation. (Figure 15 continues on page 31)

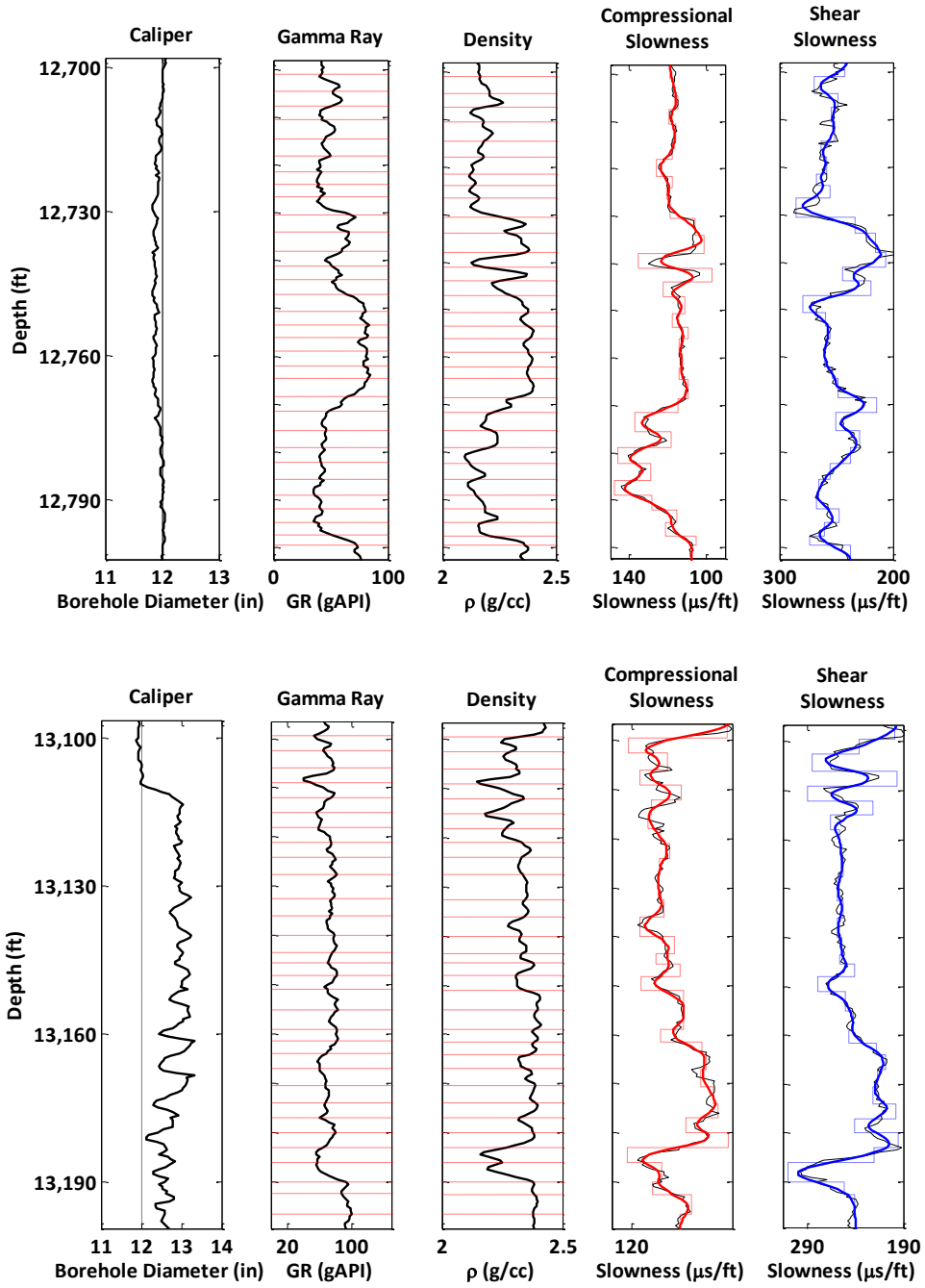

Fig. 15. Continued from page 30, (From left to right) Caliper, gamma ray, density, compressional slowness, and shear slowness logs. Red horizontal dashed lines identify the locations of bed boundaries. The second and third tracks compare noisy field logs (black) to predicted logs (blue). Dashed blocky lines with error bars describe inverted layer-by-layer slownesses of the formation.

Chapter 4: Fast forward modeling of sonic logs in deviated and horizontal wells

4.1. Introduction

Wells are drilled at high-angles to improve reservoir exposure and enhance production. However, interpretation of sonic logs in HA/HZ wells is more challenging than in vertical wells. Sonic wave propagation in a formation with thin layers is complex and not well understood by the industry. This is because as layer boundaries intercept the tool's receiver array, mode interference and conversion distort the sonic measurements (Mallan et al., 2011). Moreover, 3D numerical simulations are extremely time-consuming. Therefore, it is important to use accurate models that can fast simulate sonic logs in HA/HZ wells.

4.2. Simulation of sonic logs in deviated and horizontal wells

In previous chapters, I introduced the fast forward modeling of sonic slowness in vertical wells. However, with the prevalence of unconventional reservoirs, more wells are drilled at a high-angle or horizontally to layer boundaries; HA/HZ wells introduce challenging conditions to well-log interpretation (Passey et al., 2005). Sonic waveforms become sensitive to the presence of bed boundaries and to the contrasts in slowness between layers.

In this chapter, I perform fast forward modeling of sonic slowness in HA/HZ wells. The model is compared to 3D finite-difference simulations. Using 3D finite-difference simulations, I define the tool properties and the earth models. Simulations are done using a monopole and a dipole source. Waveforms are registered at various receivers. For the monopole source, I estimate the non-dispersive compressional mode using a modified STC method to obtain the first arrival

compressional slowness, whereas for the dipole source, I process the dispersive waveforms with a weighted spectral semblance method to obtain flexural dispersion curves.

4.3. Non dispersive modes (compressional mode)

4.3.1. Introduction

Monopole sources excite two types of waves: body waves and surface waves. In vertical wells, the compressional slowness depends on borehole-guided waves. To estimate the compressional slowness of the formation, we use the STC method on the waveforms registered at various tool receivers. However, in deviated wells the compressional slowness is influenced by both surface and converted body waves. Surface and body waves interfere with each other, which leads to amplitude variations and phase discontinuities. Consequently, we can no longer use the STC method to obtain estimations of compressional slowness. However, through numerical simulation using 3D finite-difference method and ray tracing approximations, I can show that the first arrival of the compressional mode is mostly influenced by converted body waves. Therefore, the first arrival slowness will not be affected by mode interference.

To estimate the first arrival of compressional slowness induced by converted body waves, we can simplify the problem from 3D to 1D. We can neglect the borehole because we are no longer interested in borehole-guided waves. Moreover, we can assume layers where the shear velocity is zero but the compressional velocity remains unchanged. Using this new simplified model, I obtain a faster simulation of first-arrival compressional slowness of a formation. The equations used to simulate waveforms of this simplified 1D model are described in Chapter 2.6. Once we obtain the waveforms, we use a simplified 1D-STC method to extract the first arrival compressional slowness.

4.3.2. Examples

I consider an example of two fast isotropic formations. Formation properties are shown in Table 5. The formation is penetrated by an 8-in borehole and a wireline sonic tool with an angle of 75 degrees. Two cases are considered: in the first case, the sonic source is initially in the fast formation and is logging from the faster formation *A* to the slower formation *B* while in the second case the sonic source is initially in the slower formation and is logging from formation *B* to formation *A*.

Figure 16 shows the assumed layer and tool configuration for the two cases. The tool includes a monopole source and a receiver array of 13 receivers. Each receiver station has 8 azimuthal point receivers. Figure 17 shows the azimuthal receivers of the wireline sonic tool.

	A	B
V_S (m/s)	2760	2300
V_P (m/s)	4690	4000
ρ (g/cc)	2.45	2.5

Table 5. Assumed elastic properties of formations A and B.

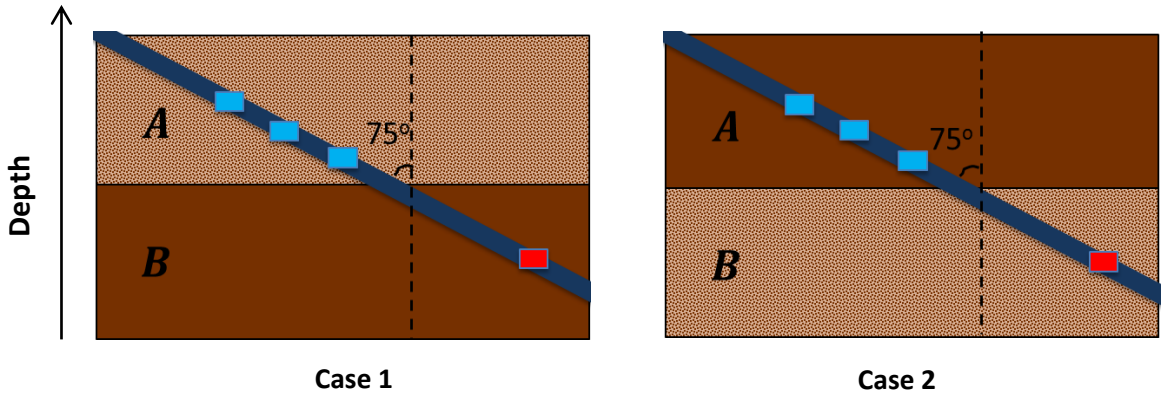

Fig. 16. Sketch of the formation and tool configuration for Case 1 (left) and Case 2 (right).

Traditionally, for a monopole source the waveform at each station of receivers is calculated by taking the average of the waveform at each azimuthal receiver. The waveform (W) at each station is therefore calculated from

$$W_i = \frac{1}{8}\sum_{n=1}^{8} W_{in}, \tag{4.1}$$

where i is the index of the station of receivers and goes from 1 to 13 and n is the index of each azimuthal receiver (from 1 to 8).

In the case of deviated borehole, we can process the receivers individually to improve the assessment of the formation. By processing all the receivers simultaneously, we can lose important information, especially near layer boundaries.

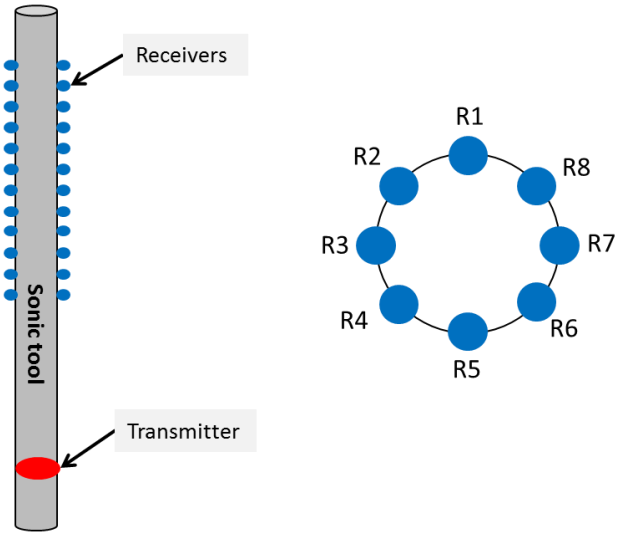

Fig. 17. Sonic tool (left) and azimuthal receivers (right). The sonic tool has 13 receiver stations and each station includes 8 azimuthal receivers.

Using numerical simulation, I show the result of processing the first arrival of the compressional mode. In Fig. 18, I compare the first arrival compressional slowness measured by the 13 receiver stations using at each station the 8 azimuthal receivers (total of 13x8 receivers) to the one I measure with the 13 receiver stations at azimuthal receiver *R3* (13x1 receivers) for the formation shown in Fig. 16, Case 2. The receiver, R3, is located on the plane of the page of Fig. 16 and below the borehole axis.

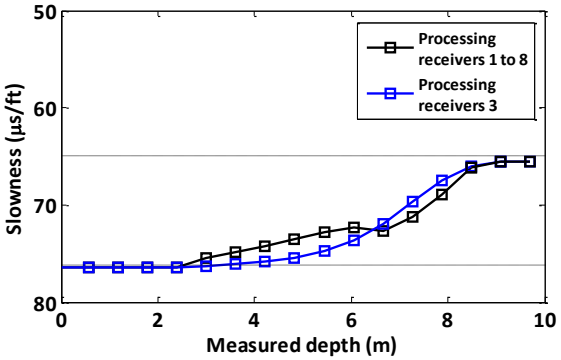

Fig. 18. Comparison of the first arrival compressional mode processed using the 8 azimuthal receiver to the first arrival compressional mode processed using only the receivers in azimuthal location R3 (previously defined), for the formation shown in Fig. 16, Case 2. Both compressional slownesses are simulated using a finite-difference method.

To take into consideration the effect of the location of receivers in the model, I adjust the model shown in Fig. 9. Figure 19 shows the new model, where, at a receiver station, each pair of receivers is separated by the borehole diameter length. I also show a sketch of the ray path, in yellow, as obtained with Snell's law from the source to receiver R3.

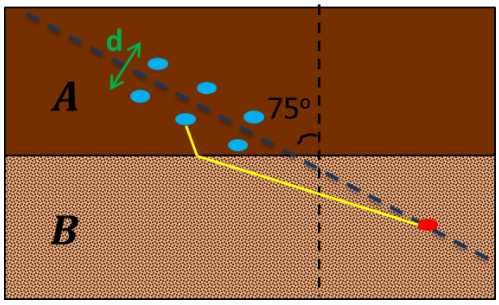

Fig. 19. Sketch of the new simplified model. Receivers are shown in blue and the source shown in red; D is the borehole diameter. The yellow line is the ray path as obtained using Snell's law.

In Fig. 20, I compare the numerically simulated first arrival of the compressional mode processed from receiver 3, to the first arrival obtained using the fast modeling. Results agree and the difference between both slownesses does not exceed 1 μs/ft. The algorithm is 1000 times faster in CPU time than conventional finite-difference methods.

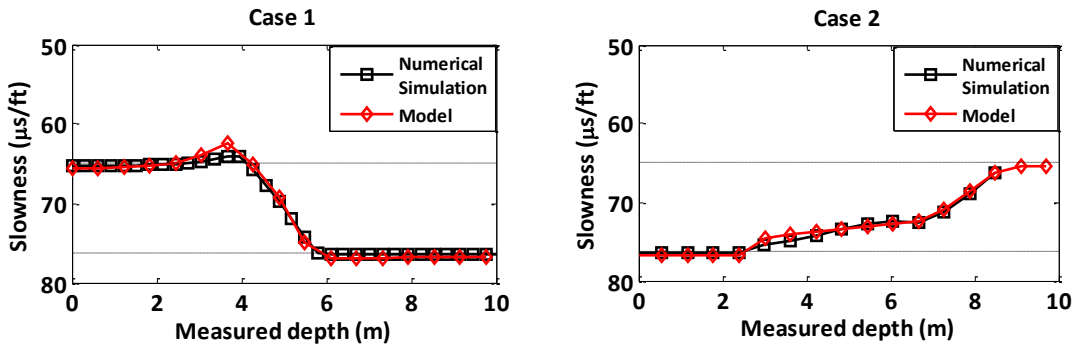

Fig. 20. Comparison of the compressional first arrival calculated using a finite-difference method to the one using the simplified algorithm, for the formation shown in Fig. 16, Case 1 (left) and in Fig. 16, Case 2 (right).

4.4. Dispersive modes (flexural mode)

4.4.1. Introduction

For the flexural mode,

i use sensitivity functions to fast forward model flexural dispersion curves. As mentioned earlier, in deviated wellbores the receiver array intercepts the layer interfaces. Consequently, mode interference occurs at low-frequencies, which makes it difficult to estimate the sonic slowness of the flexural mode. For this reason, in order to obtain accurate estimations of slowness, I only use the frequencies of the flexural mode above 4 kHz. We can extend the 2D sensitivity functions described in Chapter 2 to a 3D sensitivity function by taking into account the 3D geometry of the tool and of the formation.

To process the sonic waveform for a dipole source, I subtract the waveforms registered at two opposite sides of the receivers. Sonic tool receivers are made of piezoelectric material. They are sensitive to changes in pressure. The flux will vary as a function of $cos(\theta)$. Therefore the 3D sensitivity function is given by, $G(z, r, \theta) = G(z, r) cos(\theta)$, where $G(z, r)$ is the 2D sensitivity

function and θ is the angle between a point in the formation of coordinate (z, r) with a plane orthogonal to the center of the receiver surface.

Figure 21 shows the sensitivity function map for a dipole source. Sonic tool is shown as a gray cylinder; the source is shown in red and receivers in black. Spherical surfaces in blue, green, yellow, and red correspond to the sensitivity function at different frequency. The higher the frequency, the shorter the depth of investigation and the sensitivity is concentrated near the sonic tool.

4.4.2. Examples

I consider the same formation as in Fig. 16, Case 1 defined in Table 5. Assuming a dipole source I numerically simulate the waveforms calculated using a finite-difference method. The waveforms are then processed using the matrix-pencil method and the slowness of the flexural mode is calculated at 4 kHz, 5 kHz, 6 kHz, and 7 kHz.

Figure 22 shows the numerically simulated flexural logs with continuous lines. I then use the spatial sensitivity function method to model the flexural mode logs for the same frequencies. Logs are modeled in a few seconds of CPU time and match the numerically simulated ones.

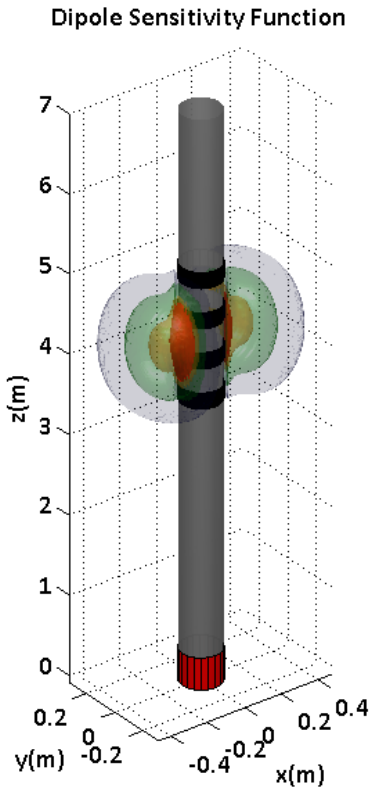

Fig. 21. Three-dimensional sensitivity function map of the flexural mode for dipole source.

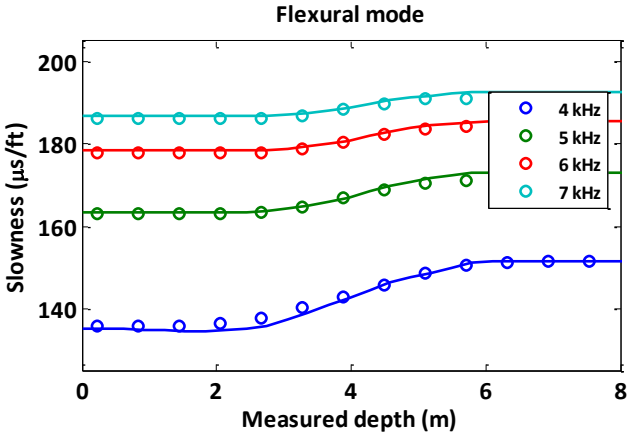

Fig. 22. Comparison of numerically simulated flexural slowness (continuous lines) to modeled slowness using sensitivity functions (circles) at 4 kHz, 5 kHz, 6 kHz, and 7 kHz for the formation shown in Fig. 16, Case 2.

Chapter 5: Conclusions

Sonic logs are an important component of formation evaluation used to determine presence of hydrocarbon reserves, presence of gas, and rock elastic properties. However, sonic logs are often contaminated with noise and are subject to averaging effects. One method to mitigate noise is sonic log inversion. However, numerical simulations of sonic logs are computationally intensive, preventing the use of inversion-based interpretation models of shear and compressional logs.

For vertical wells, I used spatial sensitivity functions to reduce the simulation time of sonic logs and implemented an inversion-based method to mitigate noise contaminating shear and compressional sonic logs. The method inverts sonic logs to estimate layer-by-layer elastic properties of rock formations, which are then used to calculate new shear and compressional logs. I showed that:

1. The vertical resolution was improved from 6 ft to 1.6 ft.
2. The simulation time was reduced by a factor of 100.
3. The spikes were mitigated.
4. The sensitivity function can be used to calculate compressional, shear, flexural, and Stoneley modes in fast and slow formations.

In deviated wells, I extended the fast modeling of the flexural mode by incorporating the 3D geometry of the formation into the sensitivity function, and I showed that:

1. The results of the fast model are accurate for the flexural mode for frequencies above 4 kHz.
2. The simulation time for high frequency flexural mode was reduced by a factor of 1000.

However, the sensitivity function cannot be used for fast simulating shear and compressional modes in deviated wells. Therefore, I used a simplified model where the presence of the borehole is neglected and the layers have zero shear velocity, and I showed that:

1. The simulation time of the first arrival of the compressional mode was reduced by a factor of 1000.
2. This method can only estimate with accuracy the first arrival of the compressional mode.

References

Aster, R. C., Borchers, B., and Thurber, C. H., 2005, Parameter Estimation and Inverse Problems, Boston, Massachusetts, Elsevier.

Chi, S. H., and Tang, X. M., 2003, Accurate approximations to qsv and qp wave speeds in TIV media and Stoneley wave speed in general anisotropic media: SPWLA 44th Annual Logging Symposium, Society of Professional Well Log Analysts, Galveston, Texas, June 22-25.

Daley, P. F., and Hron, F., 1997, Reflection and transmission coefficients for transversely isotropic media, Bulletin of the Seismological Society of America, vol. 67, no. 3, pp. 661–675.

Ellis, D., and Singer, J., 2007, Well logging for earth scientists, Springer Science & Business Media, Dordrecht, The Netherlands.

He, X., Hu, H. and Guan, W., 2010, Fast and slow flexural waves in a deviated borehole in homogeneous and layered anisotropic formations, Geophysical Journal International, vol. 181, no. 1, pp. 417–426.

Huang, S., 2015, Fast forward modeling and inversion of borehole sonic measurements using spatial sensitivity functions, Doctoral dissertation, The University of Texas at Austin, Austin, Texas.

Huang, S., Matusyzyk, P. J., and Torres-Verdín, C., 2015, Spatial Sensitivity Functions for Rapid Numerical Simulation of Borehole Sonic Measurements in Vertical Wells, Geophysics, vol. 80, no. 5, pp. D459–D480.

Huang, S., and Torres-Verdín, C., 2016, Inversion-based interpretation of borehole sonic measurements using semianalytical spatial sensitivity functions, Geophysics, vol. 81, no. 2, pp. D111–D124.

Kimball, V., and Marzetta, T. L., 1984, Semblance processing of borehole acoustic array data, Geophysics, vol. 49, no.3, pp. 274-281.

Lin, W., Wang, X., and Zhang, H., 2006, Acoustic wave propagation in a borehole penetrating an inclined layered formation, Chinese Journal of Geophysics, vol. 49, no.1, pp. 234-246.

Liu, Q., Schoen, E., Daube, F., Randall, C., Liu, H., and Lee, P., 1996, A three-dimensional finite difference simulation of sonic logging, The Journal of the Acoustical Society of America, vol. 100, no.1, pp. 72-79.

Lowe, M. J., 1995, Matrix techniques for modeling ultrasonic waves in multilayered media, Ultrasonics, Ferroelectrics, and Frequency Control, IEEE Transactions, vol. 42, no.4, pp. 525-542.

Mallan, R. K., Torres-Verdín, C., and Ma, J., 2011, Simulation of borehole sonic waveforms in dipping, anisotropic, and invaded formations, Geophysics, vol. 76, no. 4, pp. E127–E139.

Matuszyk, P. J., Torres-Verdín, C., and Demkowicz, L. F., 2010, hp-adaptive multiphysics finite element simulation of LWD borehole sonic waveforms: 80th Annual International Meeting, SEG, Expanded Abstracts, Denver, Colorado, October, 17-22.

Matuszyk, P. J., Torres-Verdín, C., and Pardo, D., 2013, Frequency-domain finite-element simulations of 2D sonic wireline borehole measurements acquired in fractured and thinly bedded formations, Geophysics, vol. 78, no. 4, pp. D193–D207.

Nolte, B., and Huang, X. J., 1997, Dispersion analysis of split flexural waves: Annual report of borehole acoustics and logging and reservoir delineation consortia, Massachusetts Institute of Technology, Earth Resources Laboratory.

Oyler, D. C., Mark, C., and Molinda, G. M., 2008, Correlation of sonic travel time to the uniaxial compressive strength of U.S. coal measure rocks: Proceedings of the 27th International Conference on Ground Control in Mining, National Institute for Occupational Safety and Health, pp. 338-346, Morgantown, West Virginia, USA, July, 29-31.

Passey, Q. R., Yin, H., Rendeiro, C. M., and Fitz, D. E., 2005, Overview of high-angle and horizontal well formation evaluation: issues, learnings and future directions: SPWLA 46th Annual Logging Symposium, New Orleans, Louisiana, June, 26-29.

Peyret, A., and Torres-Verdín, C., 2006, Assessment of shoulder-bed, invasion, and lamination effects on borehole sonic log: A numerical sensitivity study: SPWLA 47th Annual Logging Symposium, Veracruz, Mexico, June, 4-7.

Plona, T., Sinha, B., Kane, M., Bose, S., Wang, C., Pabon, J., and Zeroug, S., 2004, Identifying formation response using sonic dispersion curves: 74th Annual International Meeting of the Society of Exploration Geophysicists, SEG Technical Program Expanded Abstracts, pp. 322–325, Denver, Colorado, October 10-15.

Sayar, P., and Torres-Verdín, C., 2015, Using Sonic and Resistivity Effective Medium Theories to Quantify the Influence of Rock Fabric on the Mechanical Properties of Organic Mudrocks, Unconventional Resources Technology Conference (URTEC): San Antonio, Texas, July, 20-22.

Sinha, B. K., 1997, Sensitivity and inversion of borehole flexural dispersions for formation parameters, Geophysical Journal International, vol. 128, no. 1, pp. 84–96.

Sinha, B. K., Simsek, E., and Liu, Q. H., 2006a, Elastic-wave propagation in deviated wells in anisotropic formations, Geophysics, vol. 71, no. 6, pp. D191–D202.

Sinha, B., Vissapragada, B., Renlie, L., and Tysse, S., 2006b, Radial profiling of three formation shear moduli and its application to well completions, Geophysics, vol. 71, no. 6, pp. E65–E77.

Sinha, B. K., Simsek, E., and Asvadurov, S., 2009, Influence of a pipe tool on borehole modes, Geophysics, vol. 74, no.3, pp. E111–E123.

Souder, W. W., 2002, Using Sonic Logs to Predict Fluid Type, Petrophysics vol. 43, no. 5, pp. 412–419.

Tang, X. M., Dubinsky, V., Wang, T., Bolshakov, A., and Patterson, D., 2003, Shear-Velocity Measurement in the Logging-While-Drilling Environment: Modeling and Field Evaluations, Petrophysics, vol. 44, no.2, pp. 79-90.

Tang, X. M., and Cheng, C. H., 2004, Quantitative borehole acoustic methods, vol. 24, Gulf Professional Publishing.

Yang, J., Sinha, B. K., Valero, H. P., Bose, S., and Habashy, T. M., 2011, Estimation of the formation shear and borehole fluid slownesses using sonic dispersion data in the presence of a drill collar, SEG Technical Program Expanded Abstracts, vol. 30, pp. 464–468.

Zhang, Z., Mochida, M., Kubota, M., Yamamoto, H., and Endo, T., 2010, Shear slowness estimation by inversion of LWD borehole quadrupole mode: SEG Technical Program Expanded Abstracts, vol. 29, pp.528–532.